Chapter 5

Forward detectors

5.1 Zero Degree Calorimeter (ZDC)

5.1.1 Introduction

The number of participant nucleons is the observable most directly related to the geometry of A-A collisions. It can be estimated by measuring the energy carried in the forward direction (at $0°$ relative to the beam direction) by non-interacting (spectator) nucleons. In ALICE, spectator nucleons are detected by means of Zero-Degree Calorimeters (ZDC). If all the spectators are detected, the number of participants is given by:

$$
\begin{aligned}
E_{\text{ZDC}}(\text{TeV}) &= 2.76 \times N_{\text{spectators}} \\
N_{\text{participants}} &= A - N_{\text{spectators}}
\end{aligned}
$$

where $2.76\,\text{TeV}$ is the energy per nucleon of the Pb beam at the LHC. However, such a simple estimate is no longer valid at a collider since not all the spectator nucleons can be detected (see section 5.1.2.2). The centrality information provided by the ZDC is also used for triggering at Level 1 (L1). Finally, the ZDC being also a position-sensitive detector, can give an estimate of the reaction plane in nuclear collisions.

5.1.2 Detector layout

In ALICE two sets of hadronic ZDCs are located at 116 m on either side of the Interaction Point (IP). In addition, two small electromagnetic calorimeters (ZEM) are placed at about 7 m from the IP, on both sides of the LHC beam pipe, opposite to the muon arm (see figure 5.1).

Spectator protons are spatially separated from neutrons by the magnetic elements of the LHC beam line. Therefore, each ZDC set is made by two distinct detectors: one for spectator neutrons (ZN), placed between the beam pipes at $0°$ relative to the LHC axis, and one for spectator protons (ZP), placed externally to the outgoing beam pipe on the side where positive particles are deflected. The ZN and ZP are installed on lifting platforms, in order to lower them out of the horizontal beam plane (where the radiation levels are highest) when not in use (see figure 5.2).
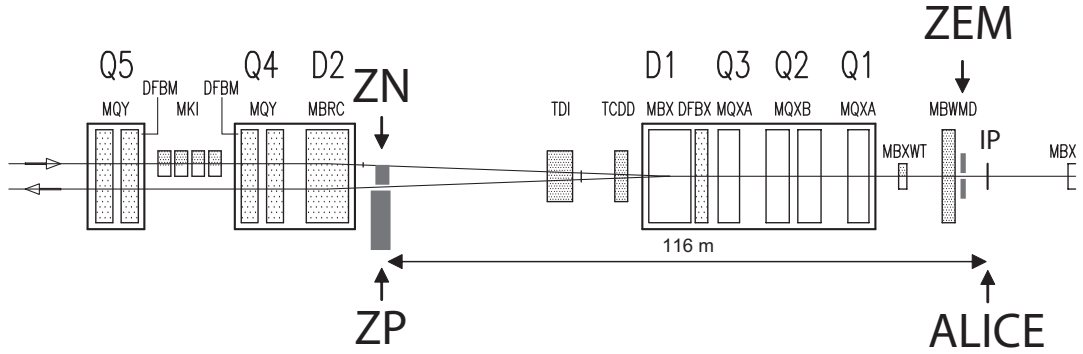
Figure 5.1: Schematic top view of the side of the ALICE beam line opposite to the muon arm. The locations of the neutron (ZN), proton (ZP) and forward electromagnetic (ZEM) calorimeters are shown. The position of the beam line dipoles (Dx) and quadrupoles (Qx) are also indicated.
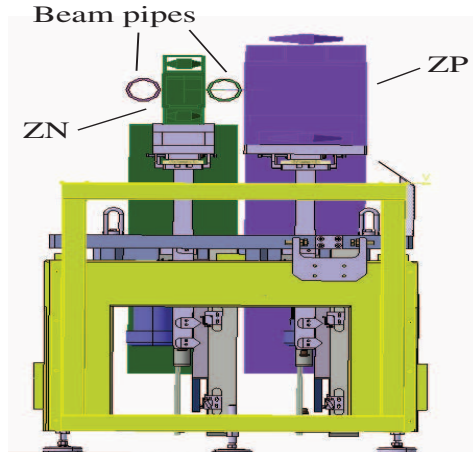

Figure 5.2: Front view of one ZDC set placed on the lifting platform in data-taking position.

5.1.2.1 Hadron calorimeters

The hadronic ZDCs are quartz fibres sampling calorimeters [169]; the shower generated by incident particles in a dense absorber (the so-called 'passive' material) produces Cherenkov radiation in quartz fibres ('active' material) interspersed in the absorber.

Due to the small amount of available space (particularly for the neutron calorimeter, whose transverse size can not be larger than 7 cm), the detectors are very compact. For this reason a very dense W-alloy was used as passive material for ZN, to maximise the containment of the showers. For the proton calorimeter there are no such stringent space constraints; moreover, the spectator proton's spot has a wide spatial distribution [10, 170]. Therefore, a larger detector made out of brass was constructed [171].

The passive material is a stack of metallic plates, grooved along the beam direction; quartz fibres are placed inside the grooves. The fibre spacing is smaller than the radiation length of the absorber, in order to avoid electron absorption in the passive material leading to non-uniformity
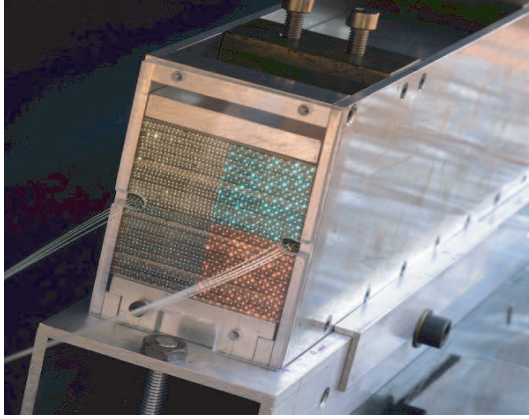
Figure 5.3: Front face of the ZN calorimeter; the quartz fibres connecting the monitoring laser system to PMTs are visible.

Figure 5.4: Front face of the ZP calorimeter.

Table 5.1: Dimensions and main characteristics of the detectors.

	ZN	ZP	ZEM
Dimensions (cm^3)	$7.04 \times 7.04 \times 100$	$12 \times 22.4 \times 150$	$7 \times 7 \times 20.4$
Absorber	tungsten alloy	brass	lead
ρ_{absorber} (g cm^{-3})	17.6	8.5	11.3
Fibre core diameter (μm)	365	550	550
Fibre spacing (mm)	1.6	4	not applicable
Filling ratio	1/22	1/65	1/11
Length (in X_0 units)	251	100	35.4
Length (in λ_{I} units)	8.7	8.2	1.1
Number of PMTs	5	5	1

in the response. The optical read-out is divided into four independent towers. One out of every two fibres is sent to a single PMT, while the remaining fibres are sent to four PMTs, each one collecting the light from a single tower. The fibres emerge from the rear face of the calorimeter, are gathered together in bundles, and routed toward the PMTs, which are located 50 cm from the end of the calorimeters, out of the beam horizontal plane. The front faces of the ZN and ZP can be seen in figure 5.3 and 5.4, respectively. Table 5.1 summarizes the main characteristics of the detectors (further details can be found in [10]).

The ZDCs will operate in a harsh radiation environment, up to 10^4 Gy/day at a luminosity of 10^{27} cm^{-2} s^{-1}. For this reason, quartz fibres were chosen, due to their intrinsic radiation hardness [172, 173]. In particular, we have used fibres with a pure silica core, silica fluorinated cladding and a hard polymer coat. Their numerical aperture is 0.22.

Cherenkov calorimeters are known to provide a very fast signal, due to the intrinsic velocity of the emission process, and have very low sensitivity to induced radioactivity thanks to their threshold behaviour.

Therefore, the limiting factors for their rate capability are the time response of the light detectors and the cable length. Beam tests with the ZN have shown that the FWHM of the detector signal, at the output of a Hamamatsu R329-02 photomultiplier tube (PMT), is of the order of 5 ns. After 200 m of low-loss cable, we estimate a FWHM of less than 20 ns. Given the expected collision frequency of 8 kHz for Pb-Pb hadronic collisions, or even the much higher rate of the electromagnetic dissociation process (predicted to be of the order of 0.1 MHz), we do not foresee any pile-up in the ZDCs.

The physics performance of the detector is related to the resolution on the number of spectator nucleons hitting the calorimeters, which in turn depends on the energy resolution of the ZDCs. Tests of the ZN were performed with a hadron beam at the SPS, at energies between 50 and 150 GeV. The calorimeter resolution, as a function of energy, is given by $(\sigma/E)^2 = (2.57 \pm 0.03/\sqrt{E(\text{GeV})})^2 + (0.103 \pm 0.006)^2$ [174]. Extrapolating this result to LHC energy (2.76 TeV) we get an expected resolution of $\sim 11.4\%$. For ZP, beam tests provided a resolution given by $(\sigma/E)^2 = (2.37 \pm 0.02/\sqrt{E(\text{GeV})})^2 + (0.125 \pm 0.002)^2$, leading to $\sigma \sim 13\%$ at LHC energy [175]. All these results are in fair agreement with detailed simulations performed within the AliRoot offline framework, see chapter 6.4.

Thanks to its segmentation, the ZN measures the position of the centroid of the incoming spectator neutrons. The resolution on the impact point of a 100 GeV hadron hitting the front face of the calorimeter is ~ 3 mm [176]. A similar resolution is expected at LHC energy. When the number of spectator nucleons increases, a significant improvement is expected.

Finally, the expected resolution on the measurement of the Pb-Pb collision impact parameter, based on the aforementioned simulation, is of the order of 1 fm [177].

5.1.2.2 Electromagnetic calorimeter

In very peripheral A-A collisions, a significant number of spectator nucleons is bound into fragments having a charge-to-mass ratio similar to the one of Pb. These fragments stay in the beam pipes and therefore cannot be detected by ZDCs. As a consequence, we can have a small amount of energy in the ZDCs for central events, where the number of spectators is small, but also for very peripheral events.

To distinguish the two classes of events, two electromagnetic calorimeters (ZEM) complement the hadronic ZDCs. They measure, event by event, the energy of particles emitted at forward rapidity (mainly photons generated from π^0 decays). Since this energy increases monotonically with the collision centrality, its value can help discriminating between central and peripheral collisions.

The detection technique is similar to the one used for the hadronic calorimeters: the absorber is made of 40 lead plates, each one 3 mm thick, with quartz fibres sandwiched in layers between the plates. The fibre cores have a diameter of 550 μm and the active to passive volume ratio is about 1/11. The ZEM fibres and plates are oriented at $45°$ with respect to the LHC axis. This choice maximises the detector response, because Cherenkov light production has a pronounced peak around $45°$ [172]. An air light guide positioned on top of the detector collects the light from the fibres up to a photomultiplier.

The calorimeter dimensions are $7\times7\times20.4\,\text{cm}^3$, and the total absorber length amounts to 35.4 X_0. In this way showers generated by impinging particles are fully contained [178] in the calorimeter which covers the pseudo-rapidity range $4.8< \eta <5.7$.

The energy resolution of the ZEM was estimated with simulations using the HIJING [142] event generator. The results show that in central collisions ($b < 2\,\text{fm}$) the total incident energy on the two electromagnetic calorimeters is about 7 TeV, while in peripheral interactions ($b \sim 10\,\text{fm}$) it is of the order of 1.5 TeV. A resolution:

$$\frac{\sigma}{E} = \frac{0.69}{\sqrt{E(\text{GeV})}}$$

has been obtained with a detector prototype tested at SPS energies. Extrapolating this resolution to the LHC conditions, we expect an energy resolution $< 1\%$ for central collisions, increasing up to 1.8% for peripheral events. Central events can be selected by requiring a small amount of energy in the hadronic calorimeters and a significant energy deposition in the ZEMs.

5.1.3 Signal transmission and readout

The analogue signals from the calorimeter's PMTs are transmitted through 215 m long low-loss coaxial cables to the closest counting room. They are then fanned out, sending an output to the trigger logic and another one to the readout chain. For the trigger, signals from the ZDCs and the ZEMs are summed separately and then discriminated. An appropriate combination of these signals will provide three ALICE L1 triggers, defining different centrality intervals (central events, semi-central events, and minimum bias events). For the readout, each analogue signal from the photomultipliers will be sent to commercial ADC modules hosted in a VME crate. When a Level 0 (L0) trigger is received, the ZDC readout electronics will start to convert the signals and make them available for the ALICE DAQ if a L1 trigger is received.

5.1.4 Monitoring and calibration

Two monitoring procedures are implemented for the ZDCs. The first is based on the detection of cosmic rays crossing the absorber material, by means of scintillators placed above and below the calorimeters. These events induce a very small amount of Cherenkov light, that may give a single photoelectron signal in the PMTs. With appropriate statistics, it is possible to measure the single photoelectron peak, directly related to the PMT gain.

The second procedure is based on a pulsed laser source. A small bunch of fibres sends the laser light to a subsample of the fibres inside the calorimeter. The peak of the resulting amplitude distribution from the calorimeters' PMTs depends on the PMT gain and on the light transmission efficiency of the fibres. Another fibre brings the light directly to a reference PMT, monitoring the stability of the laser. With these two procedures it is possible to monitor both the PMT gain and the light transmission efficiency in the fibres, which is expected to deteriorate with the radiation dose.
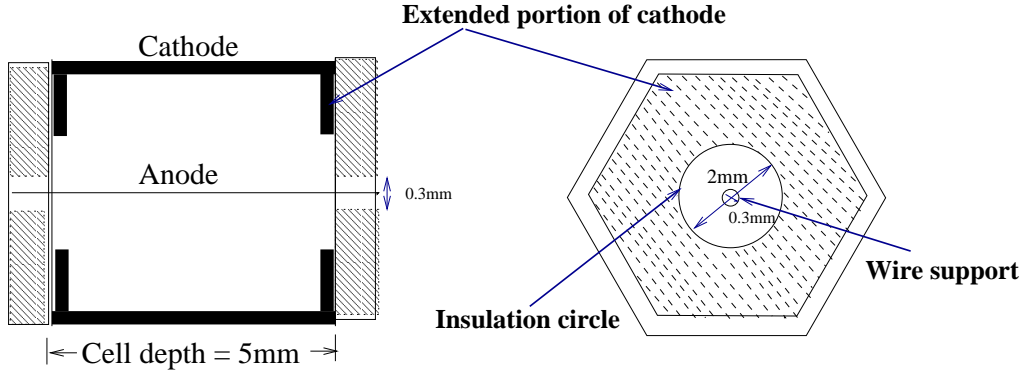
Figure 5.5: Schematic diagram of the cross section of a unit cell of the PMD.

5.2 Photon Multiplicity Detector (PMD)

5.2.1 Design considerations

The multiplicity and spatial $(\eta - \phi)$ distribution of photons in the forward pseudo-rapidity region of $2.3 \leq \eta \leq 3.7$ are measured by the Photon Multiplicity Detector (PMD) [13]. These measurements also provide estimations of transverse electromagnetic energy and the reaction plane on an event-by-event basis. The measurement of photon multiplicity gives important information in terms of limiting fragmentation, order of phase transition, the equation of state of matter and the formation of disoriented chiral condensates.

Because of the large particle density in the forward region, calorimetric techniques for photon measurements are not feasible. The PMD uses the preshower method where a three radiation length thick converter (1.5 cm thick lead with a 0.5 cm stainless steel backing) is sandwiched between two planes of highly granular gas proportional counters. The granularity and the converter thickness are optimized for high particle density so that the overlap of photon showers is minimal. The information from the detector plane placed in front of the converter is used as charged particle veto (CPV) and the preshower data from the second detector plane is used for photon identification.

The sensitive element of the detector consists of large arrays of gas proportional counters in a honeycomb cellular structure. The basic detector design was based on a detailed simulation which took into account the proper electrical field configurations within the chamber, the interaction of the particles in the gas and the generation of signals and reconstruction of physics observables. The basic cell is a honeycomb shaped cathode extended towards a 20 μm thick gold-plated tungsten wire kept at a ground potential at the centre of each cell. The schematic diagram of the unit cell is shown in figure 5.5.

The granularity of the PMD was optimised given the requirements of low occupancy, and high efficiency and purity of photon detection, on an event-by-event basis, at the maximum predicted charge particle multiplicity density ($\mathrm{d}N_{\mathrm{ch}}/\mathrm{d}\eta = 8000$). The cell cross-section and depth are $0.22\,\mathrm{cm}^2$ and $0.5\,\mathrm{cm}$ respectively, optimised on the basis of detailed simulation and test beam results. The diameters of the insulation circle and the wire support are $2\,\mathrm{mm}$ and $0.3\,\mathrm{mm}$, respectively.

The response of the detector to charged particles was studied using a $5\,\mathrm{GeV}/c$ pion beam. The left panel of figure 5.6 shows the efficiency of the detector as a function of the detector oper-
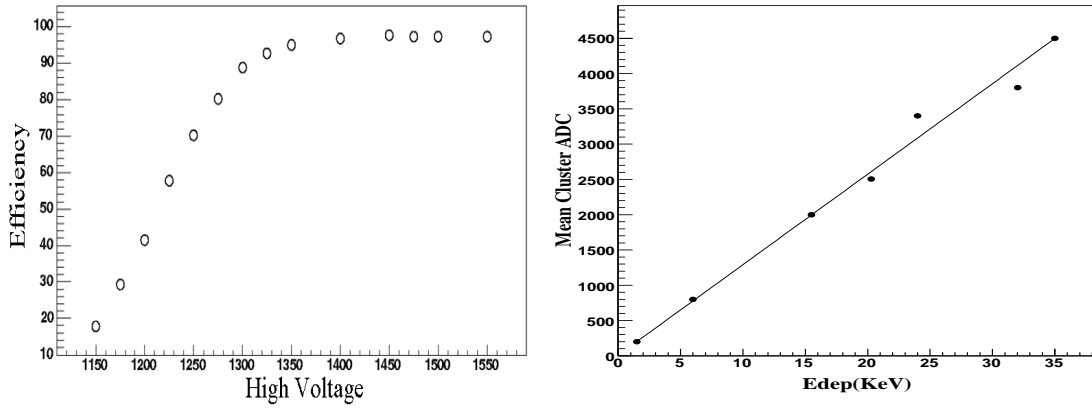
Figure 5.6: Left panel: efficiency of PMD module for charged particles as a function of operating voltage. Right panel: calibration relation between the energy deposition in terms of the measured mean cluster ADC counts versus the calculated values (in keV) for the preshower plane.

ating voltages. The optimal operating voltage for the detector is -1400 Volts which forms part of the plateau region of the proportional zone. The efficiency is about 96% for charged pions at this voltage.

The calibration of the preshower PMD was obtained by performing an energy scan with electron beams in the range 1–5 GeV and using Pb converters of different thicknesses. This is required to produce simulated data in ADC units in which the effects of the detector and readout electronics are properly folded in. The right panel of figure 5.6 shows the calibration relation for an operating voltage of 1400 Volts. The response of the detector is linear in the studied range of the energy deposition.

5.2.2 Detector layout

The PMD chambers are fabricated in the form of modules consisting of 4608 honeycomb cells. Each module is a gas tight enclosure and care is taken for high voltage isolation of each of the modules. Each plane of the PMD is made up of 24 modules as shown in figure 5.7. Two different types of modules (A-type and B-type) are employed, consisting of an array of 48×96 honeycomb cells configured in two different arrangements. Figure 5.8 shows the photographs of the two types of modules. Each module is served by separate high voltage and low voltage supplies.

The PMD is assembled in two equal halves. Each half has independent cooling, gas supply and electronics accessories. The PMD is supported from a stainless steel girder which forms part of the baby space frame in the forward region, provision being made for both $x-$ and $z-$ movements. The two halves can be moved on the girder to bring them together (as shown in figure 5.7) for data taking operation or separated for servicing. The girder itself can be moved on the baby space frame to insert the PMD in the solenoid magnet.

Table 5.2 gives an overview of PMD parameters.
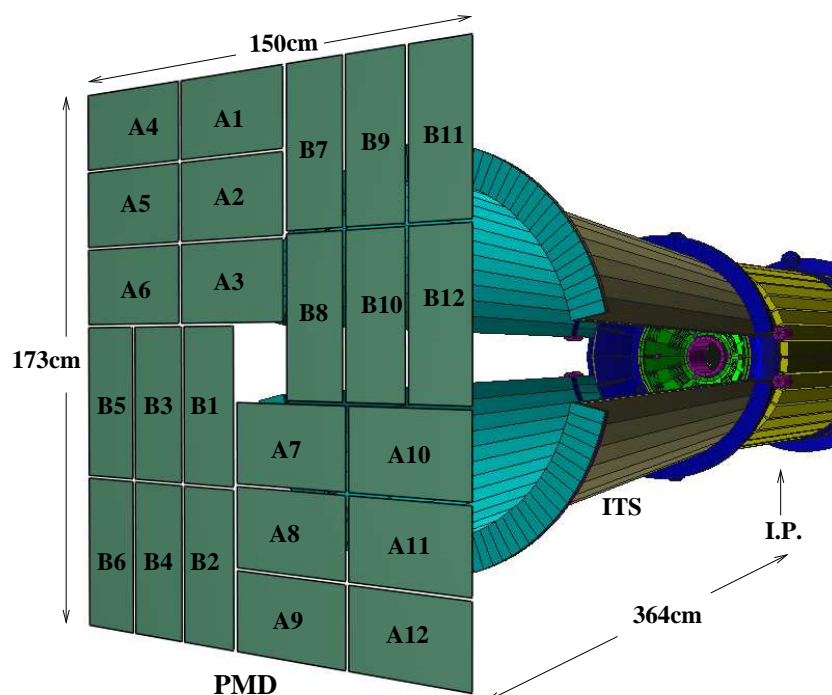
Figure 5.7: The PMD position and layout in ALICE shown with respect to the ITS. Each plane of the PMD is made up of 24 modules, half of which are of A-type and the other half of B-type.


Figure 5.8: Photographs of two types of PMD modules showing the boundary frames and the connectors with the FEE boards mounted.

Table 5.2: Summary of design and operating parameters of the PMD.

Pseudo-rapidity coverage	$2.3 \leq \eta \leq 3.7$
Azimuthal coverage	$360°$
Distance from vertex	$3.64\,\mathrm{m}$
Detector active area	$2.59\,\mathrm{m}^2$
Detector weight	$1200\,\mathrm{kg}$
Number of planes	two (Veto and Preshower)
Converter	$3\,X_0$ (1.5 cm Pb + 0.5 cm SS)
Hexagonal cell cross section	$0.22\,\mathrm{cm}^2$
Hexagonal cell depth (gas thickness)	$0.5\,\mathrm{cm}$
Detector gas	Ar/CO_2 (70% / 30%)
Operating voltage	$-1400\,\mathrm{V}$
Charged-particle detection efficiency	96%
Number of cells in one module	4 608
Number of modules per plane	24
Total number of cells	221184
Number of HV channels	48
Number of FEE boards	3 456
Number of CROCUS crates	6
Number of DDL channels	6
Cell occupancy for $dN_{ch}/d\eta = 8000$ for veto plane	13%
Cell occupancy for $dN_{ch}/d\eta = 8000$ for preshower plane	28%
Average photon reconstruction efficiency	54%
Average purity of photon sample	65%
Event size for $dN_{ch}/d\eta = 8000$	$0.12\,\mathrm{MB}$
Average time for one event readout	$100\,\mu\mathrm{s}$
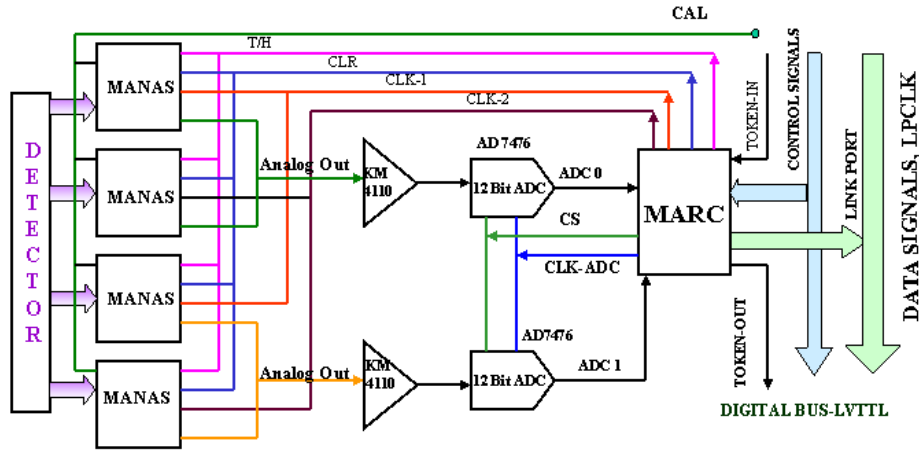
Figure 5.9: Front-End Electronics architecture of the PMD.
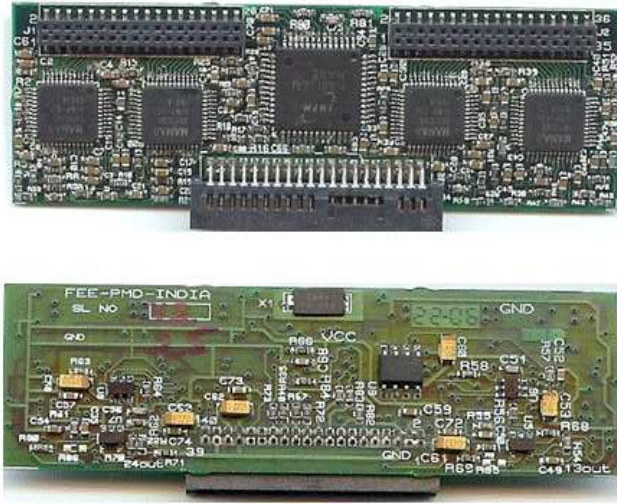
Figure 5.10: Photograph showing both sides of the Front-End Electronics board of the PMD. Four MANAS chips along with the MARC are clearly seen.

5.2.3 Front-End Electronics and readout

The schematics of the Front-End Electronics for the PMD is shown in figure 5.9, which is similar to the setup for the tracking chambers of ALICE muon spectrometer [12]. A photograph of the FEE board is shown in figure 5.10.

The signals from the anode wires for a group of 64 cells within a matrix of 4 rows and 16 columns are connected to two 32-pin FRC connectors by a flexible cable which connects to a FEE board at the other end. The signals are processed using the MANAS chip which handles 16 channels providing multiplexed analogue outputs. Each FEE board consists of four MANAS chips, two 12-bit ADCs, and a custom built ASIC called MARC chip which controls all 64 channels. The MARC chip controls 4 MANAS chips, two ADCs and performs zero suppression of the data.

A set of FEE boards are read out using Digital Signal Processors (DSP). The MARC chip communicates with DSP through 4-bit bus. The DSPs are handled through a cluster readout system (CROCUS). The main objectives of the CROCUS are to gather and concentrate the information coded on the FEE and pass to the DAQ, drive the FEE boards via patch bus controllers, receive and distribute the trigger signals, and perform the calibration of the detector. Each CROCUS crate can handle 50 patch-buses. Each patch-bus handles one chain of FEE boards.

The readout chain is designed considering the occupancies in the chains and the restrictions on chain length as dictated by faithful signal transmission. The chain arrangement for CPV and preshower planes are done differently. Each readout chain in the preshower plane has 12 FEE boards. Each quadrant of the preshower plane has a total of 36 chains and is serviced by one CROCUS crate and one DDL channel. For the CPV plane the number of FEE boards in a chain is 24 for long type modules and a mix of 24 and 12 for short type modules. The total number of chains in each half of the CPV plane is 42 and serviced by one CROCUS and one DDL channel. The total number of DDL channels for PMD is six.

5.3 Forward Multiplicity Detector (FMD)

5.3.1 Design considerations

The main functionality of the Forward Multiplicity Detector (FMD) is to provide charged-particle multiplicity information in the pseudo-rapidity range $-3.4 < \eta < -1.7$ and $1.7 < \eta < 5.0$. Figure 5.11 shows the combined pseudo-rapidity coverage of the FMD and ITS pixel detector seen from the nominal vertex position. The overlap between the FMD silicon rings and the ITS inner pixel layer provides redundancy and cross-checks of measurements between subdetectors and ensures that continuous coverage for a distribution of vertices along the z-axis. Additionally, high radial detector segmentation allows for the study of multiplicity fluctuations on an event-by-event basis while azimuthal segmentation allows for the determination of the reaction plane for each event and the analysis of flow within the FMD's pseudo-rapidity coverage.

The segmentation of the FMD was chosen such that, on average, one charged particle would occupy each strip for central events. Simulations of central Pb-Pb collisions with $dN_{ch}/d\eta \approx 8000$ in the mid-rapidity region were used to study the FMD design parameters [18]. Contributions from secondary interactions in the beampipe, ITS, T0 detector, and V0 detector as well as in services and support structures increase the number of particles impinging on the FMD. For these events, the average hit density over the whole FMD was one charged particle while no individual strip had an average hit density greater than three charged particles. Peripheral A-A collisions and pp collisions produce significantly lower hit densities. The FMD is designed to allow up to 20 minimum-ionizing particles (MIPs) in a single strip before saturating.

The segmentation chosen for the detector (strips) and the single layer geometry results from a compromise between the desired performance (multiplicity resolution) and the necessity to minimize the overall cost and complexity of the detector. The system readout time ($> 1.2\ \mu$s) does not allow the FMD to serve as a multiplicity trigger and, therefore, provides only offline analysis information.
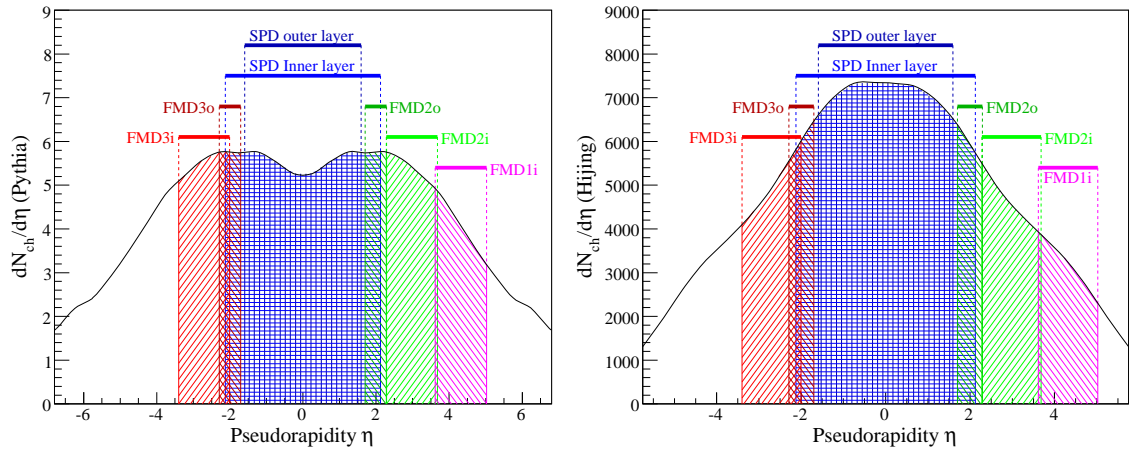
Figure 5.11: Pseudo-rapidity coverage of the FMD rings (1 inner, 2 inner and outer, and 3 inner and outer) along with the two ITS pixel layers seen from the nominal vertex position overlaid on simulated multiplicity distributions to illustrate which regions are measured by each detector. The left multiplicity distribution is produced by the PYTHIA event generator [179] with pp collisions at $\sqrt{s}$ = 14 TeV, while the right multiplicity distribution is produced by the HIJING event generator [142] with Pb-Pb collisions at $\sqrt{s_{NN}}$ = 5.5 TeV.

5.3.2 Detector layout

Figure 5.12 shows the location of each FMD ring in ALICE as well as the basic layout of the silicon sensors within an FMD ring. FMD2 and FMD3 each consist of both an inner and an outer ring of silicon sensors and are located on either side of the ITS detector. FMD2 and FMD3 are positioned to have approximately the same acceptance, however, the presence of the T0 detector necessitated a different placement for the FMD3 inner ring. Another ring, FMD1, was placed further from the interaction point opposite to the muon spectrometer to extend the charged particle multiplicity coverage. The upper limit on this additional coverage (determined to be at η = 5.0) is constrained by the increasing number of secondary particle contributions at very forward rapidity.

Each detector ring consists of 10 (for an inner ring) or 20 (for an outer ring) silicon sensors. The inner radius of the rings is constrained by the beampipe radius while the outer radius is constrained by the inner radius of the TPC. The radial span (distance from inner radius to outer radius) is limited by the 15 cm diameter wafers from which the silicon sensors are made. Two silicon sensor types were fabricated. Inner sensors consist of two azimuthal sectors each with 512 silicon strips. The radii of the inner strips range from 4.2 cm to 17.2 cm. Outer sensors also consist of two azimuthal sectors each with 256 silicon strips with radii ranging from 15.4 cm to 28.4 cm. Each ring (inner and outer) contains 10 240 silicon strips giving the full FMD a total of 51 200 silicon strips to be read out. An assembled FMD ring system (FMD3) is shown in figure 5.13. An overview of the FMD design parameters is given in table 5.3.
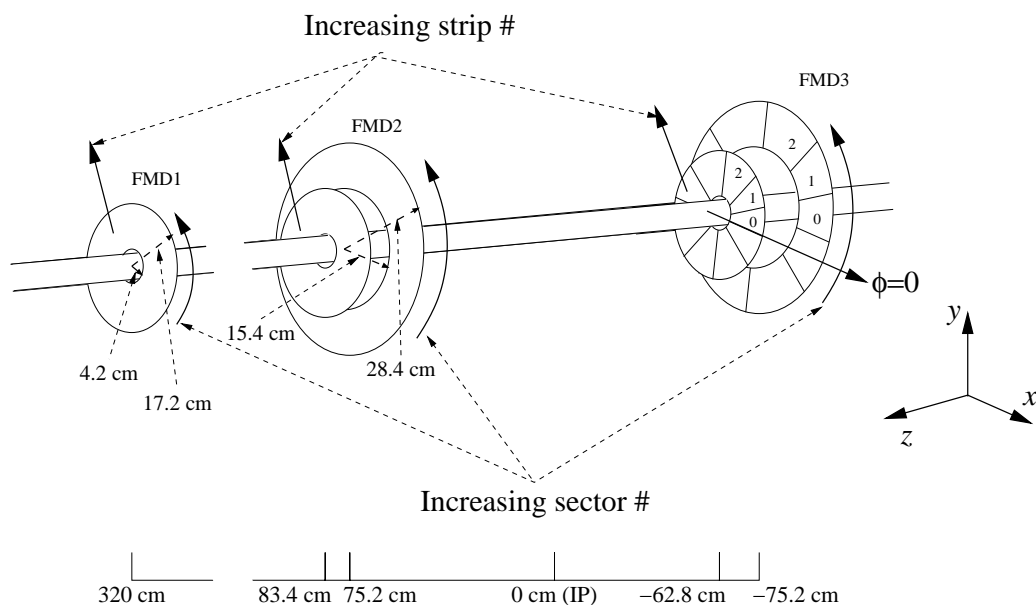
Figure 5.12: Layout of the FMD rings in the ALICE experiment. FMD3 and FMD2 are located on each side of the ITS detector while FMD1 is much further away from the interaction point (IP).

Figure 5.13: Assembled FMD3 detector. The side of the detector points away from the interaction point. Two outer digitizer boards can be seen while the two inner digitizer boards are partially covered. Each of the green cables connects a silicon module mounted on the other side of the support plate to its respective digitizer board.

Table 5.3: Overview of FMD parameters.

|	
Pseudo-rapidity coverage	$-3.4 < \eta < -1.7,\ 1.7 < \eta < 5.0$
Azimuthal coverage	$360°$
Dynamic range	0-20 MIPS
Number of ring systems	3
FMD1 geometry	inner ring
Inner ring z position	320 cm
FMD2 geometry	inner and outer ring
Inner ring z position	83.4 cm
Outer ring z position	75.2 cm
FMD3 geometry	inner and outer ring
Inner ring z position	-62.8 cm
Outer ring z position	-75.2 cm
Total channels	51 200
Dead channels	$< 0.1\%$
Number of RCUs	3 (1 per ring system)
Inner ring	(10 240 channels)
Number of digitizer cards	2
Number of sensors	10
Sensor inner radius	4.2 cm
Sensor outer radius	17.2 cm
Sector azimuthal coverage	$18°$
Azimuthal sectors per sensor	2
Strips per azimuthal sector	512
Strip pitch	250 μm
Backplane voltage	~ 75 V
VA chips per hybrid card	8
Outer ring	(10 240 channels)
Number of digitizer cards	2
Number of sensors	20
Sensor inner radius	15.4 cm
Sensor outer radius	28.4 cm
Sector azimuthal coverage	$9°$
Azimuthal sectors per sensor	2
Strips per azimuthal sector	256
Strip pitch	500 μm
Backplane voltage	~ 130 V
VA chips per hybrid card	4
Silicon sensor thickness	$325 \pm 3\ \mu$m
Silicon bulk type	n-type
Breakdown voltage	> 250 V
Leakage current per strip	$< 0.5\ \mu$A
Strip coupling capacitance	5–25 pF
Polysilicon bias resistance	~ 20 MΩ

5.3.3 Front-end electronics and readout

The signals from each silicon strip in the FMD must be collected and transferred for processing. Figure 5.14 shows the components of an inner FMD module which detects the particles and performs the initial collection of this information. A hybrid PC card with dimensions slightly smaller than the silicon sensor is attached to the sensor by gluing thin ceramic spacers between them to form a silicon module. Bonding pads exist along the perimeter of both the silicon sensor and hybrid PC card to allow small bond wires to connect the signals from the silicon sensor to readout electronics. To achieve the best signal resolution, amplification of the signal must be done as close as possible to the detector element. A VA preamplifier chip [180] is placed directly on the hybrid PC card to amplify and shape the detected signal. This preamplifier chip has low noise (250–350 ENC for the FMD detector load) and a gain allowing for signals up to 20 MIPs to be read out before saturating. Since these chips are located adjacent to the silicon detectors, they will receive the same radiation dose as the silicon detectors. The version of the VA chip used for the FMD is made with 0.35 μm AMS technology in order to resist to radiation levels well beyond 1 Mrad [181]. Each VA chip has input lines for individual amplification and shaping of 128 signals. An inner silicon module therefore requires eight VA chips while an outer silicon module requires four. A 40-pin connector on the hybrid PC card provides enough connections for power to the VA chips, control of readout, and dedicated lines for each VA chip's differential readout of the amplified signals. A separate high-voltage connector is necessary for supplying the backplane voltage to reverse-bias the silicon sensor and deplete the silicon bulk. The hybrid PC card provides filtration circuitry to reduce noise on the high voltage line. A small wire connection from the hybrid PC card is looped around the edge of the sensor and attached with conducting glue to the back side of the silicon sensor. Typical high voltage values for the inner sensors are around 75 V while outer sensors require around 130 V.

Further electronics is needed to digitize the signals and control readout. An electronics board (termed 'digitizer board') was built for this purpose. The digitizer board has the same shape as a silicon half-ring and is mounted on the backside of the low mass honeycomb support plate of the silicon modules. Short readout cables connect five inner modules to an inner digitizer card or 10 outer modules to an outer digitizer card. The digitizer card provides the low voltage to power the silicon modules as well as controlling readout. The main components of a digitizer card are the ALTRO chip [96] (three per digitizer card), each used for digitizing the signal from one or two silicon modules, and an FPGA chip, which controls the readout of the silicon modules as well as monitoring services for temperature, voltage and current.

The ALTRO chip is a fast ADC chip developed by the ALICE TPC group. It allows analogue-to-digital conversion to be done on the detector, thereby avoiding long cables for analogue signals. The use of the ALTRO chip in the FMD allows further electronics in the readout chain to be common with the TPC. An FPGA was used as a low-cost means for controlling readout and monitoring. Additionally, the use of an FPGA allows changes to be made to the readout and monitoring algorithm without having access to the physical hardware. For complicated readout procedures, such as calibration, the FPGA can be programmed.

A schematic diagram of the readout chain is shown in figure 5.15. An L0 trigger arrives directly at the board controller on the digitiser card to signify that a collision has occurred. The board controller then waits the time necessary (which is approximately 2 μs after the bunch crossing) for
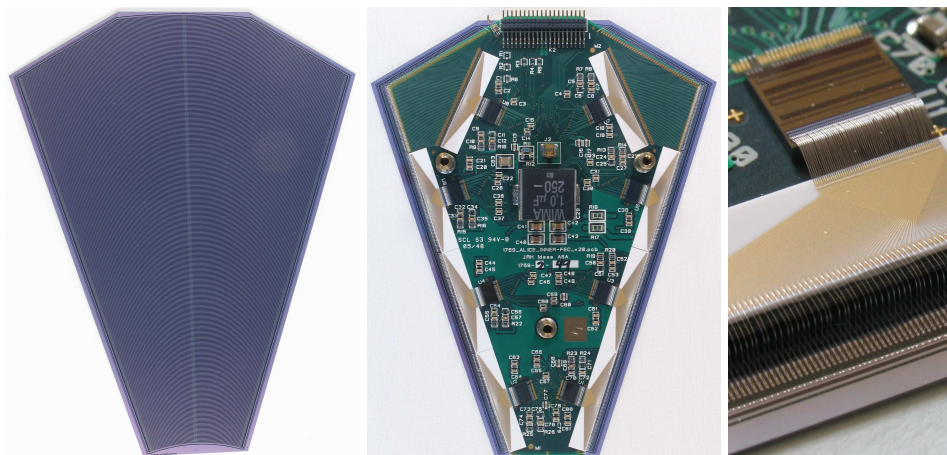
Figure 5.14: The components of an inner silicon module are shown. At left is a silicon sensor with two sectors each containing 512 silicon strips which detect charged particles via their energy loss. The middle picture shows an inner FMD silicon module where the hybrid readout card is mechanically attached to and separated from the hybrid PC card via ceramic spacers. The right-most picture is an enlarged view of the edge of this FMD module. Bond wires are attached from each strip of the silicon sensor to an input on the edge of the hybrid PC card. A pitch adapter adjusts the separation of readout lines to the separation required by the readout chip. The readout chip collects the charge from the signals deposited by the charged particles and holds the analogue value for each channel until further readout occurs.
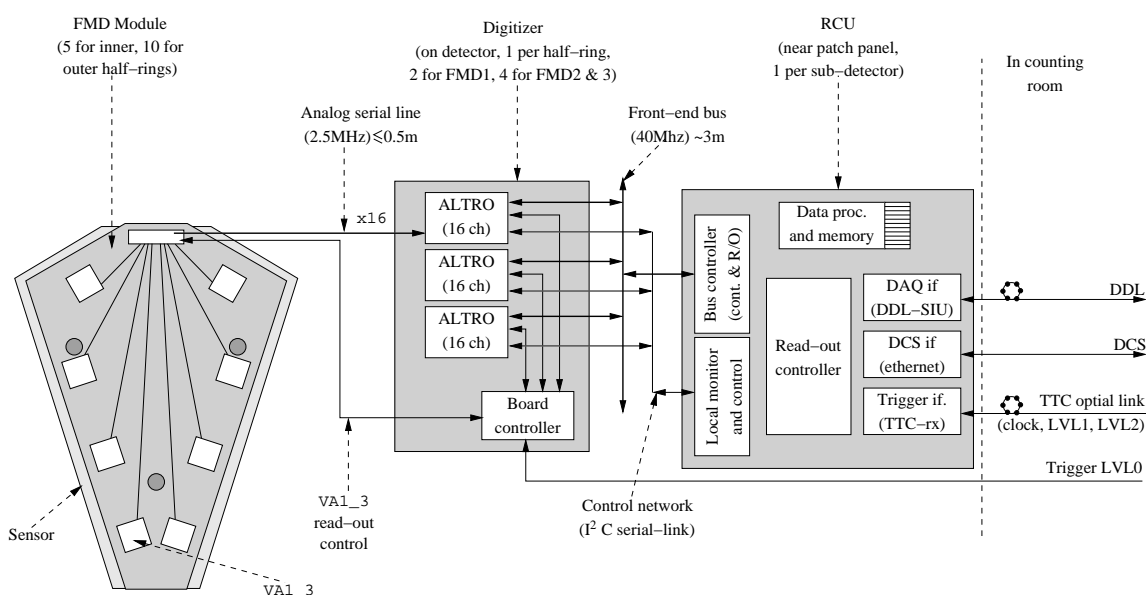
Figure 5.15: Diagram of readout chain for the FMD. The board controller on the digitizer card controls the readout sequence of the silicon modules. Analogue data is received at the ALTRO chips and digitized. The readout control unit (RCU) coordinates the transfer of the digitized data from the ALTRO chips to the DAQ system.
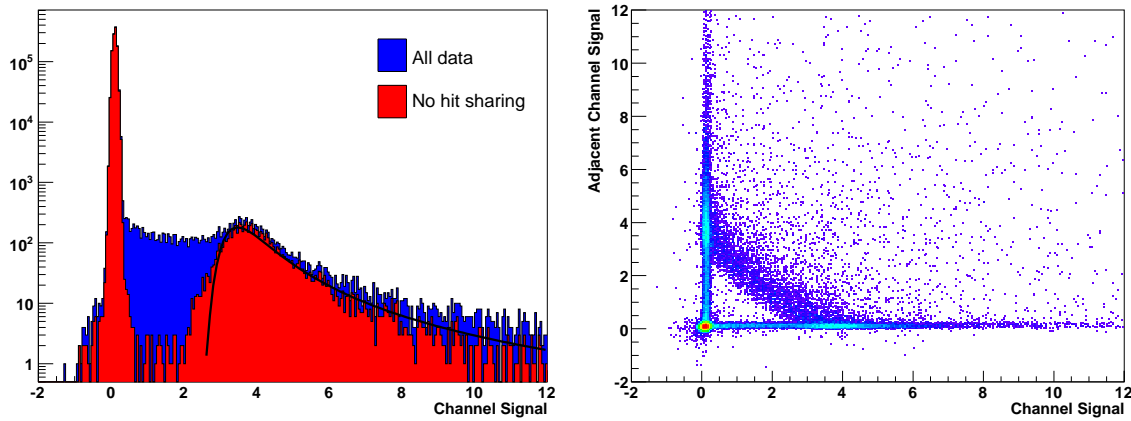
Figure 5.16: The distribution of signals from a single silicon strip is shown on the left. The blue distribution corresponds to all signals seen in that strip. A large set of signals having energies between the pedestal peak and the MIP peak is seen in this distribution. The correlation between the signal seen in this strip and an adjacent strip is shown on the right. A clear band is seen with signals whose sum of energy between the two strips is 1 MIP. These shared hits can be removed by requiring the adjacent channels to have only noise (by making a maximum energy cut) to reveal the actual detector response of Landau distributed signals (shown by the fit).

the VA chip to have the peak response after shaping of the collected signal's charge. At that time, the board controller directs all VA chips to hold the analogue levels of the signals it currently has. If the event passes the L1 criteria (approximately 6 μs after the bunch crossing), an L1 signal is sent to the board controller via the RCU [182]. The board controller then manages the serial readout of the 128 signals from each VA chip to the ALTRO where it is digitized and stored in one of four or eight buffers. Each VA chip is read out in parallel during this process. After the data has been transferred to the ALTRO buffers or if an L1 signal was never received, the hold of the analogue signals in the VA chip is released and another L0 signal can be accepted as long as there are empty ALTRO buffers. Thereafter, if the event passes the L2 criteria (on the order of 88 μs after the bunch crossing, controlled by the TPC readout time), a L2 signal is sent through the board controller to the ALTRO chips directing them to use the next buffer in the next event (if one exists). If no L2 signal is received, the ALTRO buffer is overwritten by the next event's readout. Transfer of data from the ALTRO buffers to the DAQ system is controlled by the RCU and done serially for all data in all ALTRO buffers for that event on a 40 MHz bus that can transfer data nominally at 160 MB/s and maximally at 200 MB/s.

5.3.4   Detector response

Figure 5.16 shows the calibrated response for a single FMD strip to charged particles accumulated over many events.

The large peak at zero is generated from events where no particle has deposited energy in this detector strip and the width of that peak arises from the intrinsic noise of this detector strip along with the noise accumulated during readout. While the energy per unit length deposited in a silicon detector is described by a Landau distribution, the total energy deposited in a detector strip also depends on the angle of the particle relative to the detector. Additionally, some particles share their deposited energy among multiple detector strips. After these shared hits are removed from the distribution in figure 5.16, a peak is clearly seen separated from the noise with a long tail with increasing energy. A fit of this peak to a Landau distribution yields the most probable energy loss, a minimum-ionizing particle (1 MIP), as a result. Deviations of the fit from a Landau distribution are due to incomplete removal of all shared hits. The ratio of this value to the noise (termed the signal-to-noise ratio) determines the ease of distinguishing between hit and not-hit strips. Measurements performed with the FMD [183] have shown outer sensors to have an average signal-to-noise ratio of 23:1 while inner sensors have an average ratio of 40:1, far in excess of the design criteria of 10:1.

5.4   V0 detector

5.4.1   Design considerations

The V0 detector [18] is a small angle detector consisting of two arrays of scintillator counters, called V0A and V0C, which are installed on either side of the ALICE interaction point.

This detector has several functions. It provides minimum-bias triggers for the central barrel detectors in pp and A-A collisions. These triggers are given by particles originating from initial collisions and from secondary interactions in the vacuum chamber elements. As the dependence between the number of registered particles on the V0 arrays and the number of primary emitted particles is monotone, the V0 serves as an indicator of the centrality of the collision via the multiplicity recorded in the event. Cuts on the number of fired counters and on the total charge can be applied to achieve rough centrality triggers. There are three such triggers, the multiplicity, semi-central and central triggers.

In practice and during normal operation, both arrays are required (AND mode) to provide triggers, namely: Minimum Bias trigger (MB), Multiplicity Trigger (MT), semi-Central Trigger (CT1) and Central Trigger (CT2). An OR mode can also be adopted. In pp collisions, the efficiency for the detection of at least one charged particle detected in both sides is about 75% when no secondary particle is taken into account. It raises up to 84% when the environment effects are introduced [18, 49].

Interactions of protons with the residual gas of the vacuum chamber generate tracks through the ALICE subdetectors. Minimum Bias p-Gas trigger (PG) can help to eliminate false events [184]. Moreover, a large background trigger rate is expected in the muon spectrometer trigger chambers. The absence of Minimum Bias Trigger from V0C alone (OR mode of MB trigger), is a good signal to reject a large part of these false muon triggers [185].

Finally, the V0 detector participates in the measurement of luminosity in pp collisions with a good precision of about 10%. Detailed studies can be found in [186].

Table 5.4: V0A and V0C arrays. Pseudo-rapidity and angular acceptances (deg.) of the rings.

Ring	V0A		V0C	
	η_{max}/η_{min}	$\theta_{min}/\theta_{max}$	η_{min}/η_{max}	$\theta_{max}/\theta_{min}$
0	5.1 / 4.5	0.7 / 1.3	$-3.7 / -3.2$	177.0 / 175.3
1	4.5 / 3.9	1.3 / 2.3	$-3.2 / -2.7$	175.3 / 172.4
2	3.9 / 3.4	2.3 / 3.8	$-2.7 / -2.2$	172.4 / 167.5
3	3.4 / 2.8	3.8 / 6.9	$-2.2 / -1.7$	167.5 / 159.8
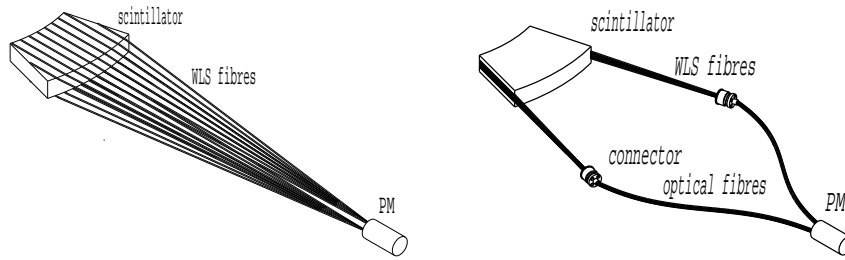
Figure 5.17: Schematic design of the V0A (left) and V0C (right) detection elements.

5.4.2 Detector layout

The V0A detector is located 340 cm from the vertex on the side opposite to the muon spectrometer whereas V0C is fixed to the front face of the hadronic absorber, 90 cm from the vertex. They cover the pseudo-rapidity ranges $2.8 < \eta < 5.1$ (V0A) and $-3.7 < \eta < -1.7$ (V0C) and are segmented into 32 individual counters each distributed in four rings (table 5.4).

Extensive tests [187] were performed to choose the best design for the elementary counters and the easiest integration of the disks in the system. The material consists of BC404[1] scintillating material (2.5 and 2.0 cm in thickness for V0A and V0C respectively) with 1 mm in diameter BCF9929A Wave-Length Shifting (WLS) fibres.[1] The fibres spaced by 1 cm are embedded in the two transverse faces of the segments following the 'megatile' technique [188] for the V0A array (figure 5.17). There are 32 elementary counters arranged in 4 rings and 8 sectors of $45°$. The fibres are grouped by layers of 9 units and glued along the two radial edges of the segments for the V0C array (figure 5.17). There are 48 elementary counters of this type distributed following two inner rings of 8 counters and two outer rings of 16 counters. The latter ones are connected 2 by 2 to make an unique detection element. A picture of each array is shown in figure 5.18.

The radiation effects on V0, located close to IP and at small angles, were of concern and investigated [189]. Results of irradiations of elements show that it could be necessary to replace some of them due to the loss of signal. Therefore, spare inner V0C elements are foreseen if large irradiation effects require their replacement.

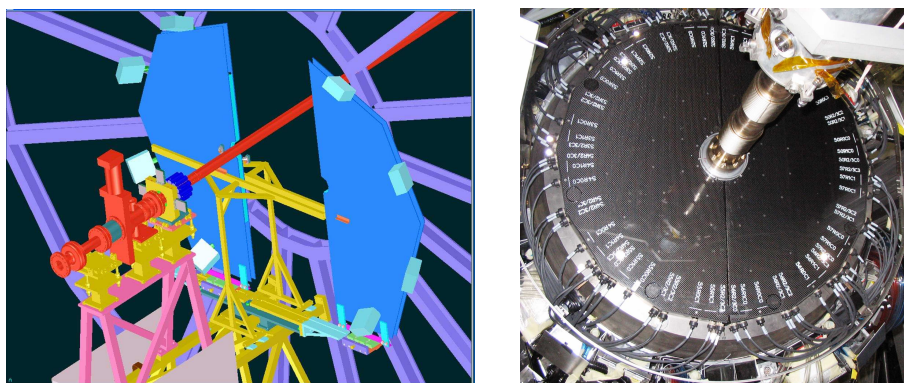The light is guided to the photo-multiplier system H6153-70MOD from Hamamatsu.[2] The

---

[1]Bicron, Saint-Gobain Industrial Ceramics, P.O. Box 3093, 3760 DB Soest, The Netherlands.
[2]Hamamatsu Photonics, 360 Foothill Rd Bridgewater, NJ 08807, U.S.A.
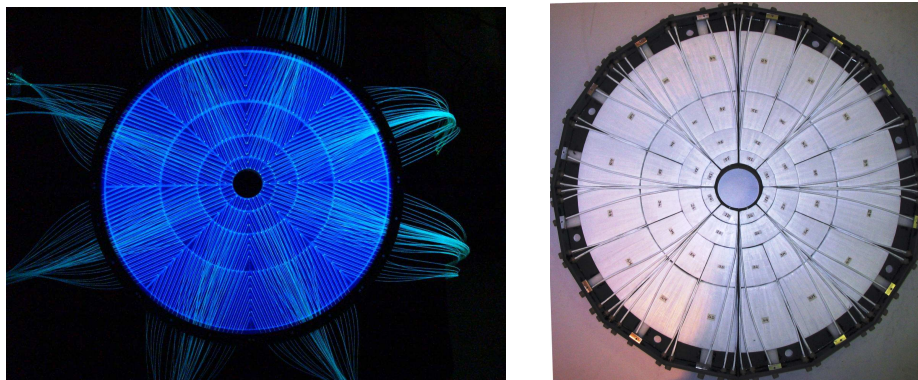
Figure 5.18: Front view of V0A (left) and V0C (right) arrays.

**Figure 5.19**: V0A 3D drawing (left) and V0C picture (right).

PMTs are fixed on the V0A disk holder in groups of 4 units and connected directly to the WLS fibres. They are installed on the absorber in groups of 8 units for the V0C and connected to counters through Mitsubishi[3] optical fibres 3.22 m long. A picture of each device is shown in figure 5.19.

5.4.3   Front-end electronics

Two signals are delivered to the Front-End Electronics (FEE). The first one is unchanged, the second one amplified by a factor 10. Signal charge and arrival time relatively to the LHC bunch clock are measured for the 32 channels of both arrays. The time resolution of the individual counters is better than 1 ns. Two types of triggers are provided from each array [18]. The first one is based on pre-adjusted time windows in coincidence with the time signals from the counters. Minimum Bias, Beam-Gas and Multiplicity Triggers are obtained by this method. The second type of triggers is based on the total charge collected by the arrays. The two Centrality Triggers are built starting from these quantities.

The readout and data acquisition architecture is designed to be compatible with the different running modes and with the trigger rates [18]. The triggers listed in section 5.4.1 and combinations of some of them, are available. Only five triggers which are chosen according to specificities of collisions and recorded data are sent to the Central Trigger Processor (CTP).

---

[3]Mitsubishi PMMA fibres distributed by Promic, 46 rue de la Pierre Plantée, 42650 Saint-Jean Bonnefonds, France.
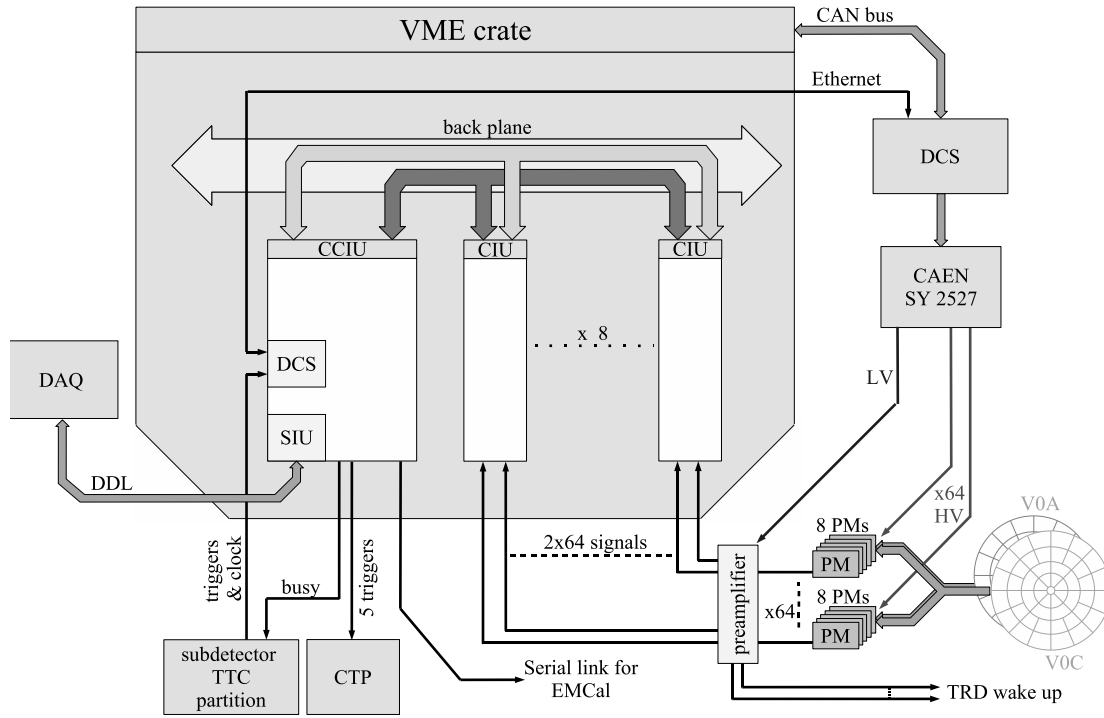
Figure 5.20: V0 Front-End Electronics architecture.

The trigger generation, readout, and data acquisition chain of the V0 consist of two types of 9U boards located in one 9U VME crate and linked by a full custom-made back plane (figure 5.20).

The Channel Interface Unit (CIU) board performs the PMT's anode signal integration (dual charge integrator), the digitization of the time, the pre-processing for the generation of the various triggers, and the data storage during a L0 and a L2 trigger. The two main components of this board are the threshold discriminator and the HPTDC [190], a Time-to-Digital Converter. Each CIU board processes anode signals from the eight photo-multipliers of a V0 ring. There are four CIU boards per array.

The Channel Concentrator Interface Unit (CCIU) board distributes the clock to elements of the FEE, generates the calibration triggers, the five final trigger and busy signals, collects and organizes the data from CIU boards, and provides several interfaces with the Experiment Control System. The three main blocks of the CCIU board are (i) the FPGA for the data handling (data collection on the back plane, data preparation for several interfaces), (ii) the SIU mezzanine, interface between DAQ and FEE, and (iii) the DCS mezzanine, interface between FEE and DCS (through an ethernet link) for the V0 slow control and between FEE and the TTC partition.

Irradiation effects were evaluated with low energy proton beam. The number of Single Event Upsets (SEU) induced in a FPGA chip was determined as a function of the flux of particles. Considering the position of the FEE in the cavern, no deterioration of electronics components is expected during 10 years of ALICE running [191].

5.5 T0 detector

5.5.1 Design considerations

The T0 detector [18, 192, 193] was designed with the following objectives: First, to generate a start time (T0) for the TOF detector. This timing signal corresponds to the real time of the collision (plus a fixed time delay) and is independent of the position of the vertex. The required precision of this signal is about 50 ps (r.m.s.). Then, to measure the vertex position (with a precision $\pm$ 1.5 cm) for each interaction and to provide a L0 trigger when the position is within the preset values. This will discriminate against beam-gas interactions. The T0 can also generate an early 'wake-up' signal to the TRD, prior to L0. In addition, T0 provides redundancy to the V0 counters and can generate minimum bias (one or both arrays hit) and multiplicity triggers (semi-central and central).

Since the T0 detector generates the earliest (L0) trigger signals, they must be generated online without the possibility of any offline corrections. The offline corrections are applied for non-trigger signals, such as the time reference for the TOF detector. The dead time of the detector should be less than the bunch-crossing period in pp collisions (25 ns).

5.5.2 Detector layout

The detector consists of two arrays of Cherenkov counters, 12 counters per array. Each Cherenkov counter is based on a Russian made fine-mesh photomultiplier tube PMT-187, 30 mm in diameter, 45 mm long. Each PMT is optically coupled to a quartz radiator 20 mm in diameter and 20 mm thick. One of the arrays, T0-C in figure 5.21, is placed 72.7 cm from the nominal vertex. Such a small distance had to be chosen because of the space constraints imposed by the front cone of the muon absorber and other forward detectors. The pseudo-rapidity range of T0-C is $-3.28 \le \eta \le -2.97$. On the opposite side of the Interaction Point (IP), the distance of the array (T0-A in figure 5.21) is about 375 cm — comfortably far from the congested central region. The T0-A is grouped together with the other forward detectors (FMD, V0, and PMD) and covers the pseudo-rapidity range of $4.61 \le \eta \le 4.92$. In the radial (transverse) direction both T0 arrays are placed as close to the beam pipe as possible to maximize triggering efficiency.

The triggering efficiency of the detector for minimum bias pp collisions, estimated by Monte Carlo simulations, is about 40% for all inelastic processes at 14 TeV. The individual efficiencies of T0-A and T0-C are 50% and 59%, respectively. The triggering efficiency in heavy-ion collisions is, due to the high multiplicities, practically 100%. The basic parameters of the T0 detector are summarized in table 5.5.

5.5.3 Fast electronics and readout

The T0 electronics consists of the front-end electronics, located close to the arrays, inside the so-called shoeboxes, and the main T0 electronics, placed inside the T0 electronic racks, already outside of the L3 magnet, close to the racks assigned to ALICE trigger electronics. All amplitude, timing and trigger signals will be digitized and stored by the ALICE DAQ.

The T0-C and T0-A arrays generate timing signals, which feed directly to the TRD, to be used as a pre-trigger 'wake-up' signal. Due to the length of the connecting cables the coincidence
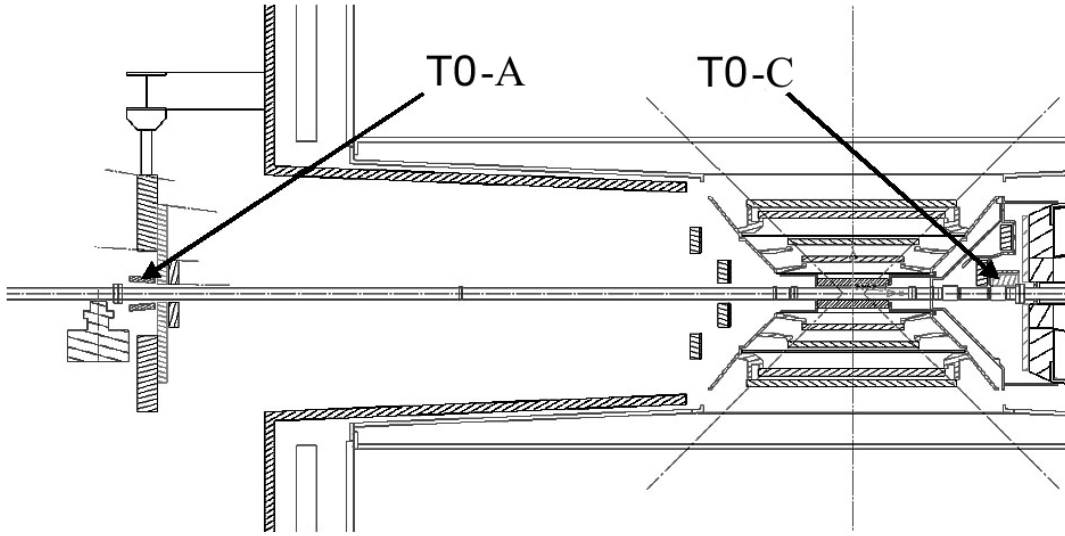
Figure 5.21: The layout of T0 detector arrays inside ALICE.

Table 5.5: Overview of the T0 detector parameters.

| Parameters	T0-A	T0-C
z-position (cm)	$+375$	-72.7
r-position (cm)	6.5	6.5
Number of Cherenkov counters	12	12
Pseudorapidity coverage	$+4.61/+4.92$	$-3.28/-2.97$
Detector active area (cm^2)	37.7	37.7
Efficiency with beam pipe (%)	50	59
Efficiency with beam pipe of both arrays in co-incidence (%)		40
Time resolution of each PMT module (ps)		37
Online vertex position resolution (cm)		1.5

requirement for the 'wake-up' is implemented not in the T0 electronic racks, but directly at the TRD level.

The T0 timing signal is generated online by a mean timer. The position of the T0 signal on the time axis is equal to $(\text{T0-C} + \text{T0-A})/2 + \text{T}_{\text{delay}}$, where T_{delay} is the fixed delay of the analogue mean timer.

The position of the vertex is measured as T0-A − T0-C and this value is sent to a digital discriminator with preset upper and lower limits thus providing the T0$_{\text{vertex}}$ trigger signal.

The T0$_{\text{semi−central}}$ and T0$_{\text{central}}$ multiplicity trigger signals are generated by 2 discriminator levels applied to the linear sum of the amplitudes from all the detectors in the array.

In order to achieve the very high online time resolution of about 50 ps, the T0 detector is equipped with sophisticated fast timing electronics [194]. The most crucial elements of the T0 electronics are: the timing discriminators, the mean timer, and the module generating T0$_{\text{vertex}}$ signal for the trigger. All these components have dead time below 25 ns, good stability and long-term
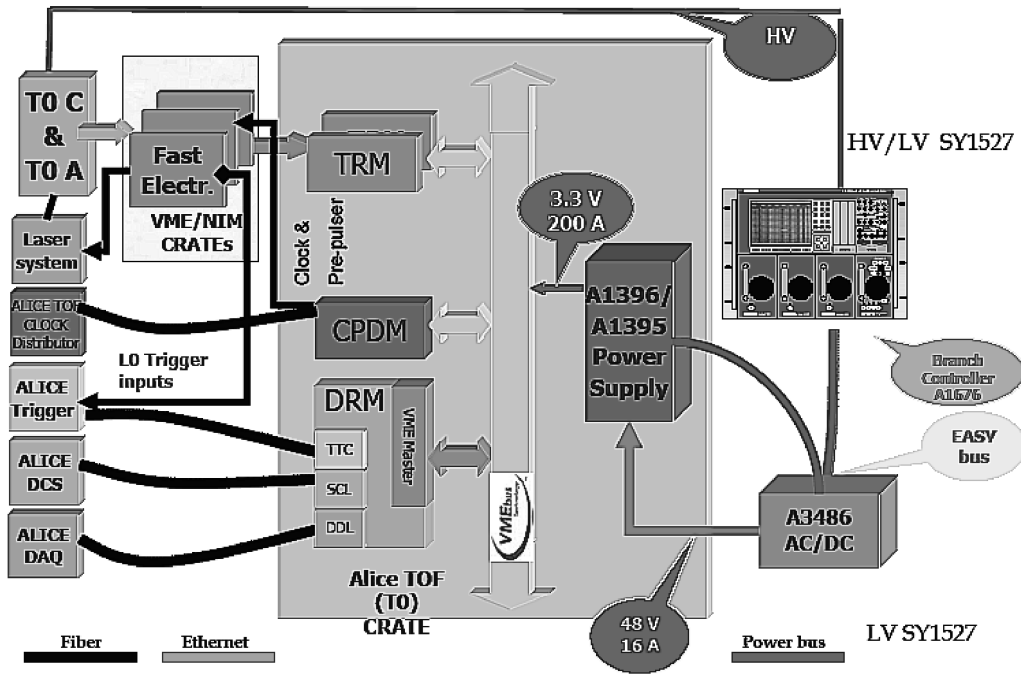
Figure 5.22: Block diagram of T0 hardware.

reliability. The modules were tested using a picosecond diode laser [195], and PS beams at CERN.

The only commercial unit in the full fast electronics chain is a Canberra Constant Fraction Discriminator model 454. It operates over the range of input amplitudes 50–3000 mV, corresponding to a dynamic range 1–60 MIP. The measured time walk, that has to be corrected offline, is 120 ps. The parameters of the mean timer and the $T0_{vertex}$ module were evaluated using two Cherenkov counters, emulating the two T0 arrays of PMTs, and 6 GeV/c negative pion and kaon beams from CERN PS. The online position of the mean timer output signal in this set-up was stable on the time axis within ± 10 ps. The time resolution of each PMT module was measured to be about $\sigma = 37$ ps. The vertex position resolution of the trigger module was also very good ($\sigma = 1.5$ cm) in the full range of allowed positions.

The readout electronics, shown in the centre of figure 5.22, consists of CPDM (Clock and Pulse Distribution module), TRM (TDC Readout Module) and DRM (Data Readout Module) cards. The CPDM card is used to distribute 40MHz low-jitter LHC clock to TRM, DRM and to main T0 electronics. The TRM card houses the HPTDC, used by T0 in very high resolution mode (24.4 ps bin width). Each TRM card contains 30 HPTDC chips. All modules are quite similar to those used for the TOF detector. The time and amplitude for each of the 24 PMTs and the main signals produced by T0 electronics (interaction time, vertex, T0-C, T0-A, linear sum of amplitudes and 2 multiplicity signals) will be stored. The DRM card is the T0 interface to the ALICE DAQ system, it reads and encodes the data from the TRM cards and sends them to the ALICE DAQ via the DDL optical link. The DRM card receives the trigger information from the CTP via the TTCrx chip and performs a slow-control function with a dedicated CPU.